Intense 1400-1600 nm circularly polarised luminescence from homo- and heteroleptic chiral erbium complexes

Received 00th January 20xx,
Accepted 00th January 20xx

DOI: 10.1039/x0xx00000x

Oliver G. Willis,[a] Andrea Pucci,[a] Enrico Cavalli,[b] Francesco Zinna *[a] and Lorenzo Di Bari *[a]

Efficient near-infrared circularly polarised luminescence (CPL) between 1400 and 1600 nm of four enantiomer pairs of homo- and heteroleptic complexes have been successfully measured. Utilising inexpensive optics and a commercial fluorimeter, discrimination of the left and right circularly polarised components was achieved, yielding remarkably high dissymmetry values in emission (g_{lum}). Most notably, homoleptic complexes $CsEr(hfbc)_4$ (hfbc = 3-heptafluorobutylyrylcamphorate) and $[TMG{-}H^+]_3Er(BINOLate)_3$ (TMG = 1,1,3,3-tetramethylguanidine; BINOLate = 1,1'-bi-2-naphtholate) show maximal $|g_{lum}|$ values of 0.83 (at 1510 nm) and 0.29 (at 1545 nm) respectively, with the former complex possessing the strongest CPL within the NIR to date.

Introduction

Chiral lanthanide complexes, in recent years, have shown interesting and unique optical and chiroptical properties,[1–16] which has made their potential implementation within chiral electronics and photonics highly desirable. In general, compounds with substantial optical activity have already shown their importance in current technologies such as circularly polarised OLEDs,[17–19] polarisation-sensitive phototransistors[20] and spin filters.[21] In particular, lanthanide chiral complexes may feature narrow emission bands, large pseudo-Stokes shifts, long lifetimes, strong circular dichroism (CD) and circularly polarised luminescence (CPL). Chiral lanthanide complexes which show strong CPL within the visible region have already been successfully employed in (bio)-assays[22–24] and within circularly polarised OLEDs.[17,25] Unlike the emission of most organic systems, the f-f transitions are not only limited to the visible region, and indeed span a wide spectral range into the near-infrared (NIR). Species which emit within the NIR and show significant chiroptical properties have potential uses ranging from biological applications[2,26] to the telecommunications industry. Indeed, Erbium, which emits around 1530 nm, is used as a dopant in current LASER systems, which are involved in the free-space long-distance optical transmission or fibre optical communications (the so-called C-band).[27,28] Besides applications of NIR luminescence in general, few reports describe CPL of Yb-based systems which emit ca. 1000 nm.[29–34] Even more rare are reports of NIR-CPL in the 1400-1600 nm range, achievable with chiral Er complexes, with only two occurrences to date.[1,3] This is likely due to the fact that instrumentation with capabilities of measuring lower energy NIR-CPL is not readily available, which in turn slows down the development of NIR-CPL active molecular compounds.

This work aims to show how our current setup in measuring Er NIR-CPL between 1400 and 1600 nm can be applied even to simple Er complexes, which are not necessarily designed for the purpose of sensitising the low energy emission.[1]

We also emphasise the interesting chiroptical features of the $^4I_{15/2} \rightarrow {}^4I_{13/2}$ transition of Er, which was predicted to show strong optical and chiroptical properties by Richardson in 1980.[35] The $^4I_{15/2} \rightarrow {}^4I_{13/2}$ transition of Er belongs within classes EI (transition dipole moment), RI (rotatory strength) and DII (dissymmetry factor), which should show relatively favourable optical and chiroptical properties compared to other lanthanide transitions.[35] From our previous work, we showed that this prediction is indeed valid, and that transitions belonging to such classes do show remarkably strong NIR chiroptical properties.[2]

Thanks to chiral lanthanide complexes possessing extraordinarily high dissymmetry factors, compared to other chiral isolated molecules (i.e., non-aggregated systems),[36–40] we were able to utilise a basic setup which requires inexpensive optical components and simple 3D-printed holders (Figure S1) to discriminate the circularly polarised components of the luminescence (Figures S7, S13 and S19). A standard commercial fluorimeter equipped with a liquid nitrogen-cooled InGaAs detector was used to collect the Er NIR emission, and the circular polarisation discrimination was achieved by 90° rotation of the quarter-wave plate (QWP), preceding a linear polariser (LP), whose axes were reciprocally oriented at ± 45°.[1]

Four enantiomer pairs of chiral Er complexes were studied, two homoleptic and two heteroleptic systems. The two homoleptic complexes were $CsEr(hfbc)_4$ (hfbc = 3-heptafluorobutylyrylcamphorate) and $[TMG{-}H^+]_3Er(BINOLate)_3$ (TMG = 1,1,3,3-tetramethylguanidine; BINOLate = 1,1'-bi-2-naphtholate) shown in Scheme 1. The former complex scaffold

---

[a] Dipartimento di Chimica e Chimica Industriale, Università di Pisa, via Moruzzi 13, 56124 Pisa (Italy). E-mail: francesco.zinna@unipi.it, lorenzo.dibari@unipi.it

[b] Department of Chemical Sciences, Life and Environmental Sustainability, University of Parma, Parco Area delle Scienze 11/a, 43124, Parma (Italy).

Electronic Supplementary Information (ESI) available: Compound preparation, instrumentation details and additional spectra. See DOI: 10.1039/x0xx00000x has been well studied across the series of lanthanides in regard to its structure and chiroptical properties.[2,12,41–43] The Eu and Yb complexes uphold the current highest g_{lum} in both the visible (+1.38 at 595 nm)[12,42] and NIR (−0.38 at 988 nm)[2], respectively. Such complexes have an antiprismatic coordination geometry, which is ideal for an efficient dynamic coupling, through which the lanthanide f-f transitions can gain sizeable rotatory strength from ligand-centred transitions.[43] The latter complex, $[\mathrm{TMG{-}H^+}]_3\mathrm{Er(BINOLate)}_3$, is the air- and water-stable analogue[44] of Shibasaki's rare earth alkali metal BINOLate (REMB), pinwheel-shaped complex.[45] The original Er Shibasaki complex was recently reported to show NIR-CPL at ca. 1550 nm.[3] In our previous work, we noted that the exchange of the alkali earth metal in the REMB complex with the organic tetra methyl guanidinium[44] causes a subtle structural rearrangement of the binaphthol ligands around the lanthanide, while still retaining an overall D_3 solution geometry.[2] The two heteroleptic complexes are formed by diketonate-based ligands as sensitisers of Er emission and the commercially available pyridine bis(oxazoline) derivatives as the chirality-inducing component. For this study, 4,4,4-Trifluoro-1-(2-naphthyl)-1,3-butanedione (NTA) acted as the Er sensitiser,[46] while 2,6-Bis(4-isopropyl-2-oxazolin-2-yl)pyridine (^{i}PrPyBox) and 2,6-Bis(4-phenyl-2-oxazolinyl)pyridine (PhPyBox) were used to provide the necessary chiral environment (Scheme 1). Similar strategies were reported for Yb and Eu CPL-active complexes.[25,26,47–49]

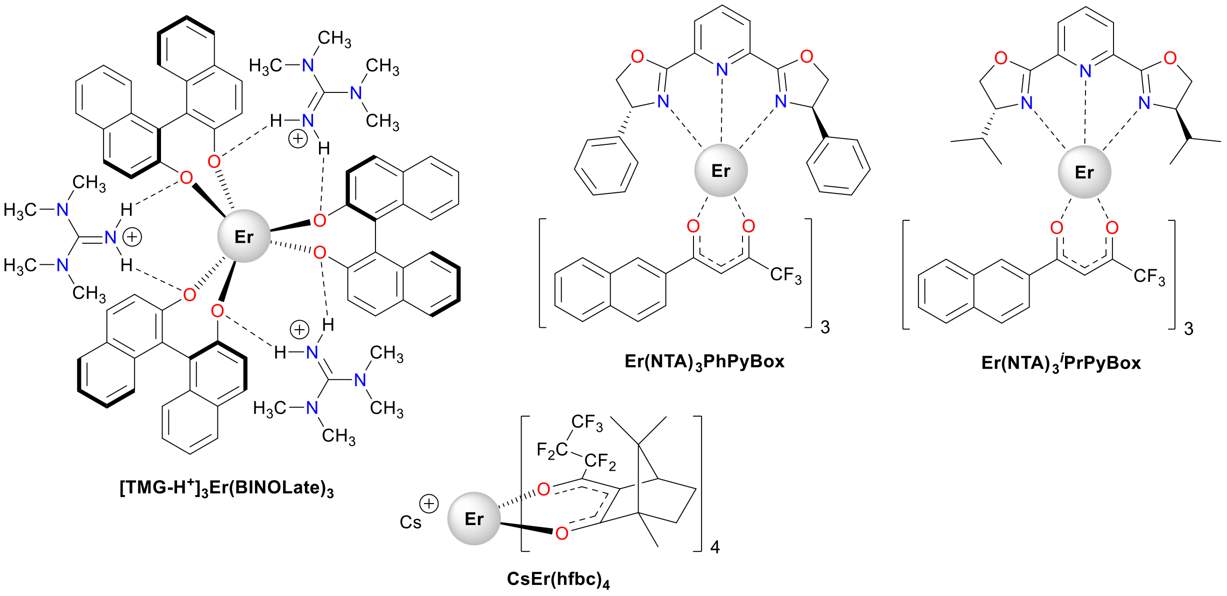

Scheme 1. Structures of the four enantiomer pairs of complexes studied in this work.

Results

CsEr(hfbc)$_4$

In THF, the CsEr(hfbc)$_4$ complex shows a UV-Vis absorption centred at 310 nm with a shoulder at lower energy (Figure S4). The excitation profile traces the low-energy shoulder with the maximum at 325 nm (Figure S3). Upon excitation, a structured emission profile is observed, containing a minimum of four distinct maxima occurring at 1477, 1509, 1530 and 1542 nm (Figure 1). Each maximum is seemingly associated to a corresponding CPL signal, which are equal and opposite for the two enantiomers (Figure 1). From high to low energy, the four predominant CPL signals have an alternating sign, e.g. −/+/−/+ for *(+)*-CsEr(hfbc)$_4$ and vice-versa for *(−)*-CsEr(hfbc)$_4$. The four distinct $|g_{\mathrm{lum}}|$ maxima occur at 1472, 1510, 1530, and 1550 with corresponding values of 0.15, 0.83, 0.08 and 0.38 (Figure S6).

The NIR-CD spectrum shows a similar sign pattern and shape as the NIR-CPL, except for the absence of a CD band at ca. 1530 nm (Figure S5). The NIR absorption spectrum shows multiple narrow emission bands of varying transition dipole intensities (Figure 1). The main CD bands occur at 1566, 1505, 1540, 1553 and 1565 nm with corresponding $|g_{\mathrm{abs}}|$ values of 0.27, 0.91, 0.40, 0.26 and 0.36 (Figure S6). Comparing these values to those previously reported for the same complex, measured in $CDCl_3$ rather than THF, we see almost identical chiroptical features, suggesting that the solvent has little impact on the structural arrangement of the ligands and electronic properties of the complex. Despite the liquid N_2 cooled InGaAs detector used for measuring the NIR emission and CPL having a sharp decrease in efficiency after 1550 nm and therefore, possible transitions present at lower energies are not observed (Figure S2), this cut-off has no impact on the g_{lum} values reported. The CsEr(hfbc)$_4$ complex shows an overall quantum yield (Q_L^{Er}) of 0.004%, measured using $\mathrm{Yb(TTA)_3(H_2O)_2}$ (TTA = thenoyltrifluoroacetone, Q_L^{Yb} = 0.35% in toluene)[50] as the reference. Despite the poor quantum yield, reliable and reproducible NIR-CPL can be measured.

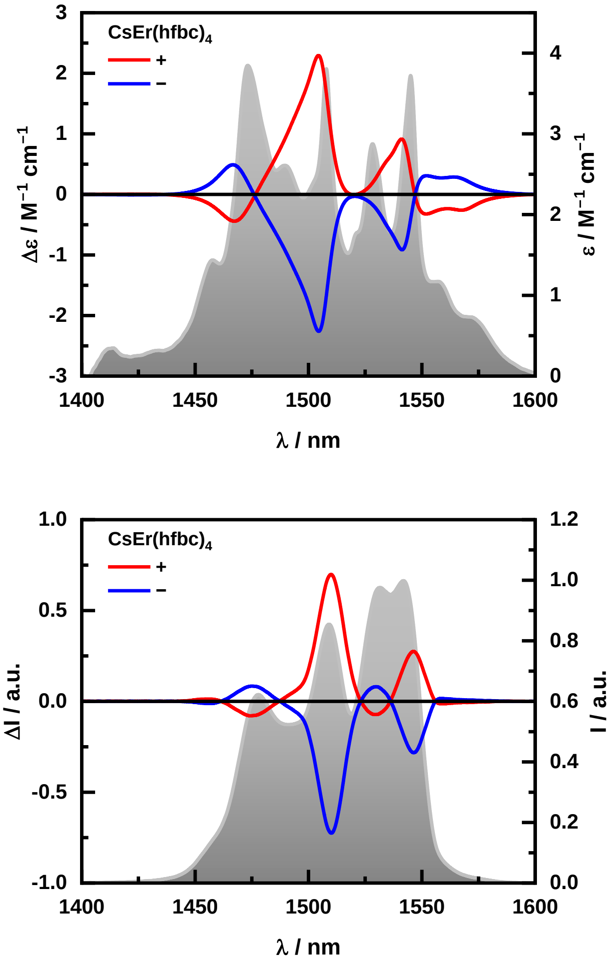

Figure 1. Top) NIR-CD spectra of CsEr(hfbc)$_4$ (16 mM) with average total absorption traced in the background (in grey). Bottom) NIR-CPL spectra of CsEr(hfbc)$_4$ (1 mM) with normalised average total emission traced in the background (in grey, λ_{ex} = 325 nm). Both spectra were recorded in anhydrous THF at room temperature.

$[\text{TMG-H}^+]_3$Er(BINOLate)$_3$

The D$_3$-symmetric, binaphtholate-based homoleptic complex $[\text{TMG-H}^+]_3$Er(BINOLate)$_3$ shows extremely rich chiroptical features, similar to the previously discussed CsEr(hfbc)$_4$. Upon ligand excitation at 365 nm (Figure S9), a weak emission profile consisting of a minimum of three major bands was observed (Figure 2). Despite the low emission intensity, the CPL was easily measured due to the complex high dissymmetry factors (Figure 2). The three low-energy major CPL bands of alternating sign at 1515, 1526 and 1545 nm give $|g_{\text{lum}}|$ values of 0.13, 0.23 and 0.29, respectively (Figure S12). The high-energy CPL band shows a $|g_{\text{lum}}|$ of 0.11 at 1455 nm. As introduced earlier, the NIR-CPL of the original Shibasaki scaffold with Er has been measured and displays dissymmetry factors similar to those reported here.[3] The $[\text{TMG-H}^+]_3$Er(BINOLate)$_3$ complex also exhibits an extremely short lifetime of ca. 0.4 µs (Figure S14).

As with the CsEr(hfbc)$_4$ complex, both the NIR-CD and NIR-CPL show remarkable similarity in terms of sign and shape, with a slightly different maxima offset (Figure S11). The NIR-CD shows an additional intense signal at 1554 nm (Figure 2) which corresponds to the highest $|g_{\text{abs}}|$ (0.71) in the entire spectra. This signal is partially lost in the NIR-CPL due to the detector cut-off (Figure S2). The four remaining intense CD bands at 1457, 1508, 1520 and 1537 nm show dissymmetry values of 0.17, 0.12, 0.43 and 0.24, respectively (Figure S12).

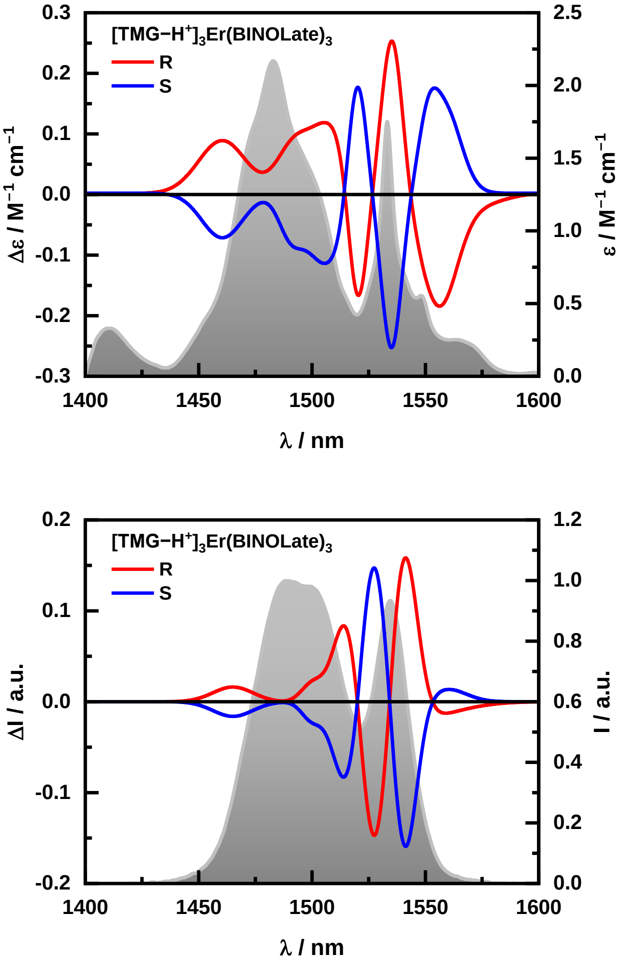

Figure 2. Top) NIR-CD spectra of $[\text{TMG-H}^+]_3$Er(BINOLate)$_3$ (26 mM) with average total absorption traced in the background (in grey). Bottom) NIR-CPL spectra $[\text{TMG-H}^+]_3$Er(BINOLate)$_3$ (1 mM) with normalised average total emission traced in the background(in grey, (λ_{ex} = 365 nm). Both spectra were recorded in anhydrous THF at room temperature.

Er(NTA)$_3{}^i$Pr/PhPyBox

Both Er(NTA)$_3{}^i$PrPyBox and Er(NTA)$_3$PhPyBox contain the sensitising ligand, NTA, which possesses a strong electronic transition centred around 345 nm (Figures S15 and S21). Upon excitation, both complexes show a single, narrow emission band with a slight shoulder at higher energy (Figures 3, S15 and S21). Er(NTA)$_3$PhPyBox shows simple chiroptical features in both NIR absorption and emission compared to the previous homoleptic Er complexes (Figure 3). The similarity between the NIR-CD and NIR-CPL is again apparent (Figure S17). The NIR-CD spectrum shows only two major bands of opposite sign occurring at 1516 and 1535 nm with corresponding $|g_{\text{abs}}|$ of 0.07 and 0.03 (Figure S18). The NIR-CPL shows a similar bisignate signal with maxima at 1523 and 1542 nm with $|g_{\text{lum}}|$ values of 0.06 and 0.02 (Figure S18).

Unlike Er(NTA)$_3$PhPyBox, the Er(NTA)$_3$^{i}PrPyBox complex shows no measurable chiroptical activity neither in absorption nor emission, despite only a simple change from the phenyl to isopropyl group. The photophysical properties for both Er(NTA)$_3$^{i}PrPyBox and Er(NTA)$_3$PhPyBox were measured and showed similar characteristics. Both complexes showed an overall quantum yield of 0.003% and lifetimes of 2.7 μs (Figures S20 and S23).

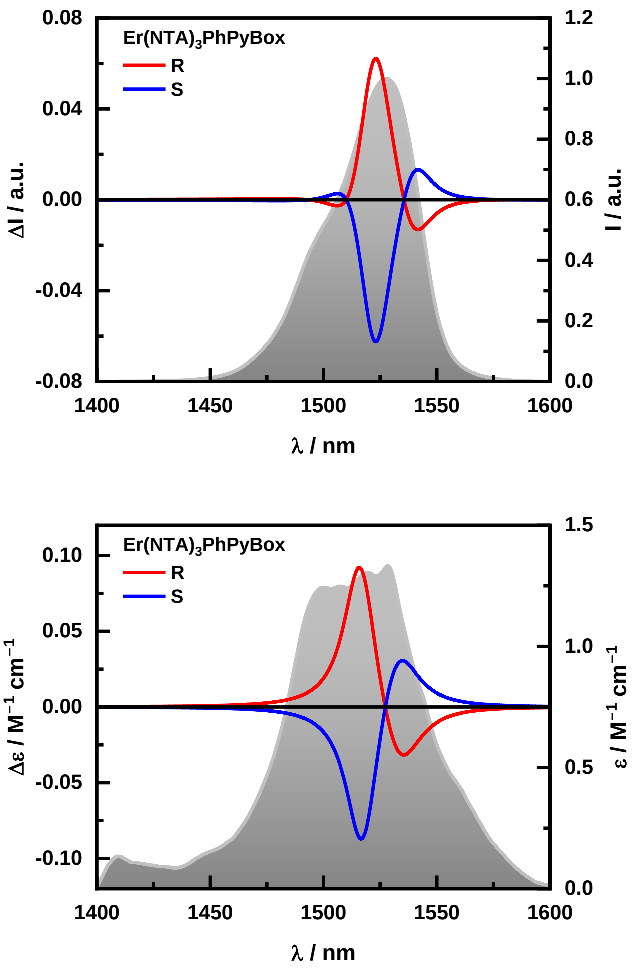

Figure 3. Top) NIR-CD spectra of Er(NTA)$_3$PhPyBox (37 mM) with average total absorption traced in the background (in grey). Bottom) NIR-CPL spectra of Er(NTA)$_3$PhPyBox (1 mM) with normalised average total emission traced in the background (in grey, λ_{ex} = 345 nm). Both spectra were recorded in anhydrous THF at room temperature.

Discussion

With overall quantum yields and emission lifetimes values in hand (Table 1), it is possible to extract valuable information about the photophysical processes involved in the emission. CsEr(hfbc)$_4$ shows an excited state lifetime (τ_{obs}) of 6.6 μs (Figure S8), significantly higher than commonly reported (optically inactive) Er compounds.[46,51,52] Assuming a radiative lifetime (τ_{rad}) of 10 msec from the literature,[51–53] an internal quantum yield ($\boldsymbol{Q_{Er}^{Er}} = \boldsymbol{\tau_{obs}/\tau_{rad}}$) of 0.07% can be calculated, as well as a sensitisation efficiency ($\boldsymbol{\eta_{sens}} = \boldsymbol{Q_L^{Er}/Q_{Er}^{Er}}$) of approximately 6%. These values may be compared to the sensitisation efficiency of 75%, and an approximately 10-times higher $\boldsymbol{Q_{Er}^{L}}$, for the extended ethynyl-PyBox Er complexes recently reported by us (Table 1).[1] This highlights the importance of the tailored antenna ligand with suitable donor states in order to efficiently sensitise the low-lying Er emissive levels. On the other hand, the particularly high τ_{obs} of CsEr(hfbc)$_4$ indicates a relatively reduced multiphonon quenching by ligand vibrational overtones, leading to an overall good CPL brightness (B_{CPL}).[54]

A higher sensitisation efficiency (10%) is obtained in the case of Er(NTA)$_3$^{i}Pr/PhPyBox complexes. The observed emission lifetime is approximately double with respect to optically inactive Er diketonates.[46,55] Finally [TMG−H$^+$]$_3$Er(BINOLate)$_3$ compounds display the shortest τ_{obs} and the lowest $\boldsymbol{Q_{Er}^{L}}$ (0.0002%), in contrast with the closely related alkali metal Er BINOLate.[3] A possible explanation could lie in the multiphonon quenching by the guanidinium N-H low-frequency oscillators in proximity of the Er centre in [TMG−H$^+$]$_3$Er(BINOLate)$_3$ complexes.

Consistently with the Yb and Eu analogue,[2,12,42] CsEr(hfbc)$_4$ exhibits the highest $|g_{lum}|$ factors among the Er complexes discussed here. In particular, the 1510 nm value (0.83) is the highest value reported for Er CPL, to the best of our knowledge. Such a value represents a 70/30 ratio of the two circularly polarised comment of the emission.

Table 1. Summary of the photophysical and chiroptical results of the four complexes studied, as well as the previously published [Er(^{i}PrPyBox-NMe$_2$)$_2$]·3OTf complex.[1]

Complex	ε / M^{-1} cm^{-1} (λ / nm)	τ_{obs} / μs	Q_{Er}^{L}	Q_{Er}^{Er}	η_{sens}	$\lvert g_{lum}\rvert$ (λ / nm)	B_{CPL} / M^{-1} cm^{-1}
CsEr(hfbc)$_4$	34830 (311)	6.6	0.004%	0.07%	6%	0.83 (1510)	0.23‡
[TMG−H$^+$]$_3$Er(BINOLate)$_3$	59279 (335)	0.4	0.0002%	0.01%	5%	0.29 (1545)	0.0005‡
Er(NTA)$_3$PhPyBox	42752 (335)	2.7	0.003%	0.03%	10%	0.06 (1523)	0.035‡
Er(NTA)$_3$^{i}PrPyBox	10246 (367)	2.7	0.003%	0.03%	10%	/	/
[Er(^{i}PrPyBox-NMe$_2$)$_2$]·3OTf§	59586 (447)	4.0	0.03%	0.04%	75%	0.33 (1539)	0.7

‡ Calculated using a modified formula (Equation S3).

§ See ref[1].

[TMG−H$^+$]$_3$Er(BINOLate)$_3$ displays $|g_{lum}|$ values in line with its alkali metal Er BINOLate analogue, despite a significantly different geometry.[3] Finally and remarkably, in the case of diketonate complexes, only Er(NTA)$_3$PhPyBox showed a significant chiroptical activity in the NIR-IR. This is at odds with the behaviour of Eu and Yb similar complexes, where the complexes bearing ^{i}PrPybox ligand displayed similar or higher CPL activity with respect to the PhPyBox counterpart.[25,26,47,49] This can be rationalised by considering that an emergent vanishing signal can be observed if transitions between M$_J$ levels are very close in energy and bear an opposite sign. This is ultimately due to the crystal field splitting induced directly or indirectly by different ancillary ligands.

In all cases, NIR-CD spectra are very similar to the corresponding NIR-CPL ones (Figures 5, 11, 17). The similarities between the NIR-CD and CPL in Er complexes are consistent with our previous observations.[1] Such behaviour stems from the fact that M_J levels of the $^4I_{15/2}$ and $^4I_{13/2}$ terms are closely spaced in energy, so that they are significantly populated at room temperature (k_BT at 300 K is 209 cm^{-1}). This has the effect that, unlike with other lanthanides, most transitions of the $^4I_{15/2} \leftrightarrow {}^4I_{13/2}$ manifold are observed both in absorption and emission and with a similar rotatory strength.[1] Note that the solutions used for NIR emission/CPL spectra have a very low optical density ($A < 10^{-3}$), thus excluding self-absorption contributions to NIR-CPL spectra.

Conclusions

We have shown that, despite low emission efficiency, NIR-CPL in the 1400-1600 nm range can be easily achieved with relatively simple Er chiral complexes, both homo- and heteroleptic ones. In particular, hfbc ligand proves its remarkable ability to induce strong CPL onto lanthanide complexes,[2] even in the NIR region. The other homoleptic complex, $[TMG{-}H^+]_3Er(BINOLate)_3$, also shows impressively strong CPL intensity, reaching $|g_{lum}|$ values of 0.29 at 1545 nm. The heteroleptic complexes show differing results. A simple exchange of a phenyl group to an isopropyl in the chiral ancillary ligand completely cancels any chiroptical properties of the complex.

Moreover, we have shown that the experimental setup for measuring NIR-CPL, which utilises inexpensive optics adapted for commercially available fluorimeters through suitable 3D-printed holders, produces reliable and repeatable results which otherwise could not be achieved by any instrumentation currently commercially available. The optical arrangement possesses great versatility and accessibility, which will hopefully inspire further research into CPL of systems endowed with high dissymmetry values. A wider accessibility of measuring capabilities and suitable complexes will hopefully open the way to novel applications of NIR-CPL emitters for bioassays and NIR CP-OLEDs.

Author Contributions

O.G.W. carried out spectroscopic measurements, data analysis and complex synthesis; A.P. gave instrumentation support; E.C. supervised lifetime measurements; F.Z. and L.D.B. conceived the idea, supervised the whole work, and discussed the data regularly; O.G.W. and F.Z. wrote the manuscript. All authors read and approved the final manuscript.

Conflicts of interest

There are no conflicts to declare.

Acknowledgements

O.G.W is grateful for the financial support from the European Commission Research Executive Agency, Horizon 2020 Research and Innovation Programme under the Marie Sklodowska-Curie grant agreement No. 859752-HEL4CHIROLED-H2020-MSCA-ITN-2019. This project has also received funding from the Italian Ministero dell'Università, PRIN 20172M3K5N. F.Z. and A.P. acknowledge financial support from the University of Pisa (PRA 2020_21).

References

1 O. G. Willis, F. Petri, G. Pescitelli, A. Pucci, E. Cavalli, A. Mandoli, F. Zinna and L. Di Bari, *Angew. Chem. Int. Ed.*, 2022, **61**, e202208326–e202208326.
2 O. G. Willis, F. Zinna, G. Pescitelli, C. Micheletti and L. Di Bari, *Dalton Trans.*, 2022, **51**, 518–523.
3 N. F. M. Mukthar, N. D. Schley and G. Ung, *J. Am. Chem. Soc.*, 2022, **144**, 6148–6153.
4 M. Deng, N. D. Schley and G. Ung, *Chem. Commun.*, 2020, **56**, 14813–14816.
5 L. Arrico, C. Benetti and L. Di Bari, *ChemPhotoChem*, 2021, **5**, 815–821.
6 P. Stachelek, L. MacKenzie, D. Parker and R. Pal, *Nat. Commun.*, 2022, **13**, 553–553.
7 C. Lincheneau, C. Destribats, D. E. Barry, J. A. Kitchen, R. D. Peacock and T. Gunnlaugsson, *Dalton Trans.*, 2011, **40**, 12056–12059.
8 D. E. Barry, J. A. Kitchen, L. Mercs, R. D. Peacock, M. Albrecht and T. Gunnlaugsson, *Dalton Trans.*, 2019, **48**, 11317–11325.
9 M. Starck, L. E. MacKenzie, A. S. Batsanov, D. Parker and R. Pal, *Chem. Commun.*, 2019, **55**, 14115–14118.
10 D. E. Barry, D. F. Caffrey and T. Gunnlaugsson, *Chem. Soc. Rev.*, 2016, **45**, 3244–3274.
11 A. T. Frawley, R. Pal and D. Parker, *Chem. Commun.*, 2016, **52**, 13349–13352.
12 J. L. Lunkley, D. Shirotani, K. Yamanari, S. Kaizaki and G. Muller, *J. Am. Chem. Soc.*, 2008, **130**, 13814–13815.
13 H.-Y. Wong, W.-S. Lo, K.-H. Yim and G.-L. Law, *Chem*, 2019, **5**, 3058–3095.
14 F. Zinna and L. Di Bari, *Chirality*, 2015, **27**, 1–13.
15 L. E. MacKenzie and R. Pal, *Nat. Rev. Chem.*, 2021, **5**, 109–124.
16 B.-A. N. Willis, D. Schnable, N. D. Schley and G. Ung, *J. Am. Chem. Soc.*, 2022, **144**, 22421–22425.
17 F. Zinna, U. Giovanella and L. D. Bari, *Adv. Mater.*, 2015, **27**, 1791–1795.
18 Y. Yang, R. C. da Costa, D.-M. Smilgies, A. J. Campbell and M. J. Fuchter, *Adv. Mater.*, 2013, **25**, 2624–2628.
19 J. R. Brandt, F. Salerno and M. J. Fuchter, *Nat. Rev. Chem.*, 2017, **1**, 0045–0045.
20 B. L. Feringa, *Acc. Chem. Res.*, 2001, **34**, 504–513.
21 R. Farshchi, M. Ramsteiner, J. Herfort, A. Tahraoui and H. T. Grahn, *Appl. Phys. Lett.*, 2011, **98**, 162508.
22 R. Carr, N. H. Evans and D. Parker, *Chem. Soc. Rev.*, 2012, **41**, 7673–7686.
23 M. Leonzio, A. Melchior, G. Faura, M. Tolazzi, M. Bettinelli, F. Zinna, L. Arrico, L. Di Bari and F. Piccinelli, *New J. Chem.*, 2018, **42**, 7931–7939.
24 J. Yuasa, T. Ohno, H. Tsumatori, R. Shiba, H. Kamikubo, M. Kataoka, Y. Hasegawa and T. Kawai, *Chem. Commun.*, 2013, **49**, 4604–4606.

25 F. Zinna, L. Arrico, T. Funaioli, L. Di Bari, M. Pasini, C. Botta and U. Giovanella, *J. Mater. Chem. C*, 2022, **10**, 463–468.

26 F. Zinna, L. Arrico and L. Di Bari, *Chem. Commun.*, 2019, **55**, 6607–6609.

27 S. Yamashita, *IEEE J. Sel. Top. Quantum Electron.*, 2001, **7**, 41–43.

28 C.-H. Yeh, C.-C. Lee and S. Chi, *IEEE Photonics Technol. Lett.*, 2003, **15**, 1053–1054.

29 C. L. Maupin, D. Parker, J. A. G. Williams and J. P. Riehl, *J. Am. Chem. Soc.*, 1998, **120**, 10563–10564.

30 C. L. Maupin, R. S. Dickins, L. G. Govenlock, C. E. Mathieu, D. Parker, J. A. G. Williams and J. P. Riehl, *J. Phys. Chem. A*, 2000, **104**, 6709–6717.

31 B. Lefeuvre, C. A. Mattei, J. F. Gonzalez, F. Gendron, V. Dorcet, F. Riobé, C. Lalli, B. Le Guennic, O. Cador, O. Maury, S. Guy, A. Bensalah-Ledoux, B. Baguenard and F. Pointillart, *Chem. – Eur. J.*, 2021, **27**, 7362–7366.

32 E. Cavalli, C. Nardon, O. G. Willis, F. Zinna, L. Di Bari, S. Mizzoni, S. Ruggieri, S. C. Gaglio, M. Perduca, C. Zaccone, A. Romeo and F. Piccinelli, *Chem. – Eur. J.*, 2022, **28**, e202200574–e202200574.

33 R. S. Dickins, J. A. K. Howard, C. L. Maupin, J. M. Moloney, D. Parker, J. P. Riehl, G. Siligardi and J. A. G. Williams, *Chem. – Eur. J.*, 1999, **5**, 1095–1105.

34 F. Gendron, S. Di Pietro, L. Abad Galán, F. Riobé, V. Placide, L. Guy, F. Zinna, L. Di Bari, A. Bensalah-Ledoux, Y. Guyot, G. Pilet, F. Pointillart, B. Baguenard, S. Guy, O. Cador, O. Maury and B. Le Guennic, *Inorg. Chem. Front.*, 2021, **8**, 914–926.

35 F. S. Richardson, *Inorg. Chem.*, 1980, **19**, 2806–2812.

36 J. Li, C. Hou, C. Huang, S. Xu, X. Peng, Q. Qi, W.-Y. Lai and W. Huang, *Research*, , DOI:10.34133/2020/3839160.

37 E. M. Sánchez-Carnerero, A. R. Agarrabeitia, F. Moreno, B. L. Maroto, G. Muller, M. J. Ortiz and S. de la Moya, *Chem. – Eur. J.*, 2015, **21**, 13488–13500.

38 K. Ma, W. Chen, T. Jiao, X. Jin, Y. Sang, D. Yang, J. Zhou, M. Liu and P. Duan, *Chem. Sci.*, 2019, **10**, 6821–6827.

39 H. Tanaka, Y. Inoue and T. Mori, *ChemPhotoChem*, 2018, **2**, 386–402.

40 Y. Nagata and T. Mori, *Front. Chem.*, 2020, **8**, 1–6.

41 D. Shirotani, H. Sato, K. Yamanari and S. Kaizaki, *Dalton Trans.*, 2012, **41**, 10557–10567.

42 J. L. Lunkley, D. Shirotani, K. Yamanari, S. Kaizaki and G. Muller, *Inorg. Chem.*, 2011, **50**, 12724–12732.

43 S. Di Pietro and L. Di Bari, *Inorg. Chem.*, 2012, **51**, 12007–12014.

44 J. R. Robinson, X. Fan, J. Yadav, P. J. Carroll, A. J. Wooten, M. A. Pericàs, E. J. Schelter and P. J. Walsh, *J. Am. Chem. Soc.*, 2014, **136**, 8034–8041.

45 H. Sasai, T. Suzuki, S. Arai, T. Arai and M. Shibasaki, *J. Am. Chem. Soc.*, 1992, **114**, 4418–4420.

46 P. Martín-Ramos, I. R. Martín, F. Lahoz, S. Hernández-Navarro, P. S. Pereira da Silva, I. Hernández, V. Lavín and M. Ramos Silva, *J. Alloys Compd.*, 2015, **619**, 553–559.

47 J. Yuasa, T. Ohno, K. Miyata, H. Tsumatori, Y. Hasegawa and T. Kawai, *J. Am. Chem. Soc.*, 2011, **133**, 9892–9902.

48 L. Armelao, D. B. Dell'Amico, L. Bellucci, G. Bottaro, L. Di Bari, L. Labella, F. Marchetti, S. Samaritani and F. Zinna, *Inorg. Chem.*, 2017, **56**, 7010–7018.

49 M. Górecki, L. Carpita, L. Arrico, F. Zinna and L. Di Bari, *Dalton Trans.*, 2018, **47**, 7166–7177.

50 S. Meshkova, Z. Topilova, D. Bolshoy, S. Beltyukova, M. Tsvirko and V. Venchikov, *Acta Phys. Pol. A*, 1999, **95**, 983–990.

51 S. W. Magennis, A. J. Ferguson, T. Bryden, T. S. Jones, A. Beeby and I. D. W. Samuel, *Synth. Met.*, 2003, **138**, 463–469.

52 Q. Sun, P. Yan, W. Niu, W. Chu, X. Yao, G. An and G. Li, *RSC Adv.*, 2015, **5**, 65856–65861.

53 G. Mancino, A. J. Ferguson, A. Beeby, N. J. Long and T. S. Jones, *J. Am. Chem. Soc.*, 2005, **127**, 524–525.

54 L. Arrico, L. Di Bari and F. Zinna, *Chem. – Eur. J.*, 2021, **27**, 2920–2934.

55 S. I. Klink, L. Grave, D. N. Reinhoudt, F. C. J. M. van Veggel, M. H. V. Werts, F. A. J. Geurts and J. W. Hofstraat, *J. Phys. Chem. A*, 2000, **104**, 5457–5468.